Design Principles for Energy-Efficient Legged Locomotion and Implementation on the MIT Cheetah Robot

Sangok Seok, Albert Wang, Meng Yee (Michael) Chuah, Dong Jin Hyun, Jongwoo Lee, David M. Otten, Jeffrey H. Lang, *Fellow, IEEE*, and Sangbae Kim

***Abstract*—This paper presents the design principles for highly efficient legged robots, the implementation of the principles in the design of the MIT Cheetah, and the analysis of the high-speed trotting experimental results. The design principles were derived by analyzing three major energy-loss mechanisms in locomotion: heat losses from the actuators, friction losses in transmission, and the interaction losses caused by the interface between the system and the environment. Four design principles that minimize these losses are discussed: employment of high torque-density motors, energy regenerative electronic system, low loss transmission, and a low leg inertia. These principles were implemented in the design of the MIT Cheetah; the major design features are large gap diameter motors, regenerative electric motor drivers, single-stage low gear transmission, dual coaxial motors with composite legs, and the differential actuated spine. The experimental results of fast trotting are presented; the 33-kg robot runs at 22 km/h (6 m/s). The total power consumption from the battery pack was 973 W and resulted in a total cost of transport of 0.5, which rivals running animals' at the same scale. 76% of the total energy consumption is attributed to heat loss from the motor, and the remaining 24% is used in mechanical work, which is dissipated as interaction loss as well as friction losses at the joint and transmission.**

***Index Terms*—Cost of transport (CoT), efficiency, energy regeneration, legged locomotion, quadrupeds robot.**

I. Introduction

ENERGY efficiency is a critical attribute that enables the successful use of legged robots in real applications. The ability to travel a long distance without recharging is crucial in tasks such as search-and-rescue and disaster response missions.

Although recent technological advances in legged robots have led to the ability to walk or run on flat and rough terrains, the energy efficiency of these robots is still notably worse than biological walkers or runners of a similar scale. The most widely used criterion for energy efficiency of legged locomotion is total cost of transport (TCoT): $= P/(WV)$, which is the ratio of the power consumption to the product of weight and velocity [2].

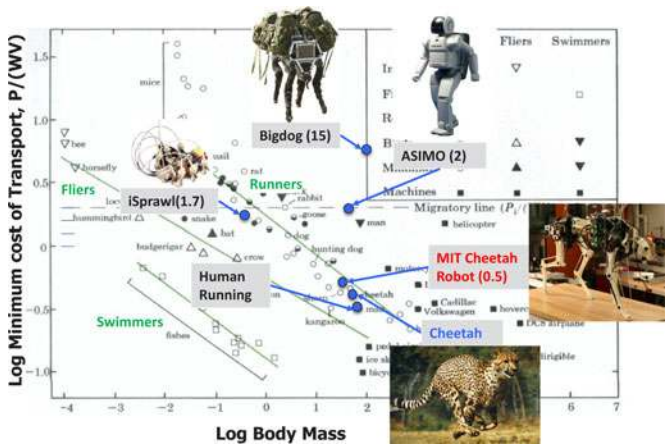

Fig. 1. Plot of TCoT versus body weight of animals and selected robots. The three classes of animal locomotion (running, flying, and swimming), occupy distinct regions of the plot. Used with permission from author of [3].

The TCoT of several robots are plotted on Tucker's animal data [3] in Fig. 1. As is shown by two of the most successful robots, the TCoT of ASIMO and Boston Dynamics BigDog are significantly higher than those of humans or animals of similar mass scale [3], [4]. Considering that the conversion efficiency in engineering actuators (e.g., from electricity to mechanical work) can be more efficient than the counterpart of the biological system (from fat to mechanical work, ranging 20%–25% [5]), there should be considerable room for improvement in current legged robots.

To date, there have been two main approaches to improve the efficiency of legged robots: passive dynamics and elastic elements. Since legged locomotion involves highly unsteady usage of actuator power and alternating positive and negative work, these approaches provide "mechanical energy capacitors" that can store kinetic or elastic potential energy and return them without consuming significant energy.

The concept of passive dynamic walking was successfully implemented in walking robots and experimentally proven to improve energy efficiency. The Cornell Ranger exploited the passive dynamics of swing legs [2], [6]: Its lowest recorded TCoT is 0.19. This locomotion efficiency is far superior to that of animals of the same scale. However, this robot sacrifices versatility in order to maximize its employment of the passive

Manuscript received August 21, 2013; revised March 29, 2014; accepted May 28, 2014. Recommended by Technical Editor R. Oboe. The preliminary version of this paper has been presented in [1]. This paper includes additional experimental results. This work was supported by the Defense Advanced Research Program Agency M3 Program.

S. Seok, A. Wang, M. Y. (M.) Chuah, D. J. Hyun, J. Lee, and S. Kim are with the Department of Mechanical Engineering, Massachusetts Institute of Technology, Cambridge, MA 02139 USA (e-mail: sangok at mit.edu; adwang@mit.edu; mcx@mit.edu; mecjin@mit.edu; jw127@mit.edu; sangbae@mit.edu).

D. Otten and J. Lang are with the Department of Electrical Engineering and Computer Science, Massachusetts Institute of Technology, Cambridge, MA 02139 USA (e-mail: otten@mit.edu; lang@mit.edu).

Color versions of one or more of the figures in this paper are available online at http://ieeexplore.ieee.org.

Digital Object Identifier 10.1109/TMECH.2014.2339013

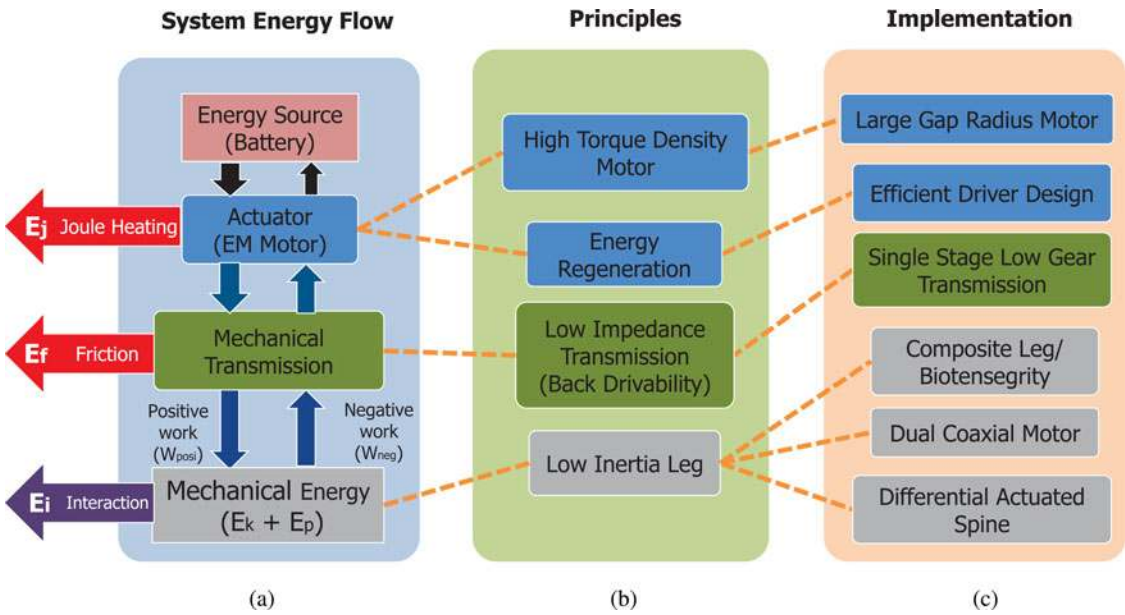

Fig. 2. (a) Energy flow diagram of the robot showing energy flows between the source and mechanical energy. Joule heating loss occurs at the motor, friction loss occurs in the mechanical transmission, and interaction loss reduces the total mechanical energy. (b) Design principles to improve efficiency at the sources of energy loss. (c) Strategies for implementing the design principles for efficiency used on the MIT Cheetah Robot.

dynamics of human walking, and so its locomotion is restricted to a particular speed in fairly flat terrain, whereas ASIMO and BigDog are highly versatile [2].

Several robots employ series elastic actuators to utilize the energy recovery of mechanical springs [7], [8] and successfully demonstrated stable locomotion. One of the most efficient robots using this method successfully is iSprawl [9]. It achieved a TCoT of 1.7, which matches animals efficiency as shown in Fig. 1. However, this robot sets the stiffness of the series elastic spring for a 14-Hz stride frequency. Because iSprawl is incapable of changing stiffness, it becomes less stable in lower frequency running. One way to solve this problem is to use additional small actuators [10] dedicated for stiffness adjustments, but this can result in increased system complexity, extra weight, and additional energy consumption.

Another approach that utilizes elastic energy storage is employing parallel mechanical springs [11]. Instead of adding mechanical springs in series, this approach suggests finding an optimum stiffness and no-load position for springs in parallel with joint actuators. The idea was implemented in a dynamic simulation of a bounding quadruped model, and the results show that employing parallel springs can reduce the total power consumption by 15%, and, if switchable springs are implemented, by 53%.

Similarly, the system approach has been previously explored in morphological computation to exploit the intrinsic dynamics of the robot for legged locomotion [12]–[14]. Because the energy exchange through these mechanical elements is governed by passive dynamics, these approaches tend to be tuned for only a narrow range of speeds. Furthermore, these approaches are intended to minimize mechanical work and often do not directly address the entire energy loss, significant part of which is attributed to nonmechanical loss such as heat.

In order to develop energy-efficient robots more effectively, we need to understand the energy loss mechanisms associated with the entire system. Robotic designers should consider every energy flow stage shown in Fig. 2 to calculate overall energy dissipation. Energy efficiency is one of the most frequently used cost functions in optimizing control parameters in legged robots. However, the optimization processes in the literature often use only the mechanical cost of transport as a cost function, which is smaller compared with other energy dissipation modes such as Joule heating of coils in electromagnetic actuators and transmission loss. Such approach provide a incomplete solution for optimum efficiency, considering that mechanical cost of transport contributes only a fraction of the total cost of transport [15] [16], as shown in several robots (Scout II: MCoT/TCoT=0.34 [15], Cornell Ranger: MCoT/TCoT=0.21 [17], ATRIAS: MCoT/TCoT=0.24 $\sim$ 0.4 [18], MIT Cheetah: MCoT/TCoT=0.24 [1]). Furthermore, there have been few discussions on minimizing energy loss caused by actuators and few design methodologies or comprehensive design principles to maximize locomotion efficiency. It has been noted that the characteristics of actuation systems not only govern dynamic behavior but also characterize the energy flow in the robot. Therefore, there are opportunities to improve efficiency by optimizing actuator and mechanism design as a whole system.

It is remarkable that the term “efficiency” in locomotion represented by TCoT is inherently different from the generic concept of efficiency used in a machine: The ratio of input power to output power. The locomotive system does not have an output power if they travel on relatively flat ground, because the net change of the mechanical energy of the system is zero. The

entire amount of energy reduced at the energy source is dissipated through locomotion. Therefore, locomotion in general is an energy dissipative process, and losses occur throughout the energy flow path from energy source to interactions with the environment. This is why the denominator of the TCoT is a product of the magnitudes of two orthogonal vectors (mass times gravity times horizontal speed) instead of a dot product of two vectors, which would yield zero.[1]

Considering that legged locomotion is an inherently dissipative process and the energy dissipative mechanism of a robotic system is highly dependent on the operation condition, conventional design approaches to higher energy efficiency do not necessarily yield a solution for more efficient locomotion. For example, machine designers often choose the actuator and gear ratios based on the torque requirement and the maximum efficiency speed. Since the speed–torque curve of running is highly variable and highly dependent on many aspects including the dynamics of the running gait, the dynamics of the transmission and actuator, and the control algorithms. In particular, the transmission ratio plays a crucial role in the overall leg impedance and control bandwidth.

In order to provide design insights for developing energy-efficient robots, this paper introduces design principles for achieving high energy efficiency by analyzing energy loss throughout the entire system: actuator loss, transmission loss, and interaction loss. The next section explains these three energy loss mechanisms in legged locomotion and proposes design principles that can minimize the losses. Section III introduces how the design principles are implemented in the MIT Cheetah robot. Section IV demonstrates various experimental results and shows the system performance by comparing the cost of transport of the MIT Cheetah robot with animals and other robots. Finally, Section V discusses the conclusions and future work.

II. Design Principles for Efficiency

In arriving at practical design principles for energy efficiency in legged robots, understanding energy flow is a critical step. It is important to analyze every possible pathway by which energy flows within a robot during locomotion. In Fig. 2, the leftmost column represents the energy flow of the robot. The three main energy-loss mechanisms in the flow are described later. The first loss is heat loss at the force transducer. In an electromagnetic (EM) motor, this is largely comprised of Joule heating, $E_j = \int I^2 R dt$, where I is the current and R is the motor terminal resistance; a minor component is the parasitic amplifier switching loss. The second is transmission loss, E_f. In a typical robot, this includes all losses through force transmission paths, such as friction losses at gears, belts, and bearings. The third energy-loss mechanism is interaction loss, including all the losses caused at the system boundary, which is the interface between the robot and the environment. Major sources of this loss in legged locomotion are foot impacts and air drag. The design of the robot needs to consider all of these factors to minimize overall loss.

[1]For the same reason, we use miles-per-gallon to represent the fuel economy of a car, instead of efficiency as a percentage.

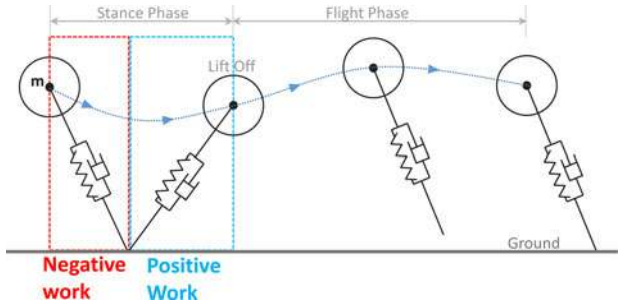

Fig. 3. Energy Regeneration as it occurs in a SLIP model. During landing, there is deceleration, which charges the battery, and during jumping, the battery supplies the energy for acceleration.

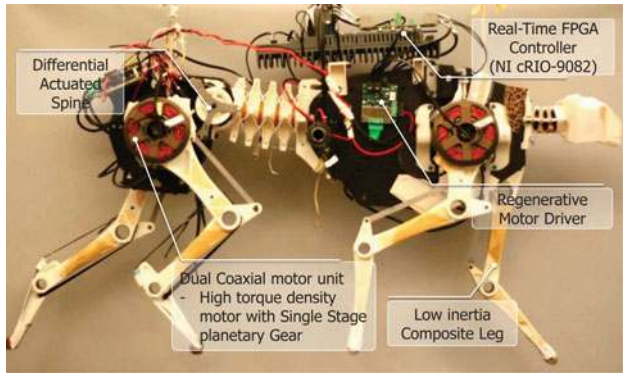

Fig. 4. Side view of the MIT Cheetah Robot showing design principles as implemented in hardware.

We propose four design principles essential to the design of efficient legged robots. These principles shown in Fig. 2(b) directly address the three losses as denoted by the dotted lines. It is important to note that these design principles are guidelines that can be used to minimize individual losses independently from others. A truly optimized robot would consider the interactions between all design parameters for which there are too many to consider.

A. Principle 1:High Torque-Density Motor

This design principle suggests employing high torque-density EM motors for minimizing energy loss in actuators. This principle directly concerns the Joule heating of the EM motor by reducing the required electric current to provide torque for the locomotion. Here, the term torque density refers mass-specific continuous torque. If we assume the heat dissipation characteristic[2] of the motor remains same, the continuous torque of the motor represents how much torque the motor can generate at a constant heat dissipation. Then, the continuous torque is directly related to motor constant ($K_M = \tau/\sqrt{I^2 R}$), which represents torque per Joule heating power. For example, if the torque density of the motor doubles without changing other

[2]The continuous heat dissipation power capability of the motor is dependent on the thermal resistance and the temperature difference between of the motor and environment; we assume this value does not change if the motor mass is similar.

factors such as the mass of the motor and heat dissipation characteristics, the Joule heating E_j can be reduced by 75%. In general, if the design parameters of the motor is optimized for the torque density, the coil mass increases and the stator steel mass decreases, which results in low peak torque. The motor should be designed also considering the maximum torque of the locomotion cycle, where the torque-electric current relationship starts becoming nonlinear due to magnetic flux saturation. At a given torque requirement, therefore, increasing the torque density of the EM motor is highly desirable for efficient locomotion without compromising the dynamics of the system.

B. Principle 2:Energy Regeneration

As discussed earlier, legged locomotion involves dynamic bidirectional energy flow from the energy source to the interaction with the ground. In legged locomotion, even in steady-state running, there are periods in each stride in which the leg does negative work [19]. These periods include the beginning of the ground phases and the ending of the swing phase, where the torques and angular velocities are in the opposite direction to each other. Fig. 3 illustrates this concept for the SLIP model. Similar to the regenerative braking in electric cars, it is desirable to recover that energy rather than dissipating it in dampers and brakes [20].

Such energy recovery can be done by employing series elastic actuation. An elastic element is placed between the actuator and the end effector that can temporarily store and release energy from the ground contact. If the stiffness of the spring is well tuned for the natural dynamics of the body given by the running speed, this method can achieve very high theoretical efficiency with the actuator injecting a small amount of energy to account for impact losses.

Instead of utilizing the mechanical spring and damper, if virtual impedance is realized by electromagnetic torque control at the actuators, a part of the energy generated from negative work is recovered by electric regeneration, as demonstrated in electric cars. In this case, the parameters of virtual impedance (e.g., stiffness and damping coefficient) can be programmed in arbitrary form and adjusted instantly in a wide range starting from nearly zero impedance. Unlike mechanical damping that would dissipate all energy, the virtual damping impedance does not represent the energy dissipative element; it partially returns energy back to the source.

Efficient energy regeneration requires enhanced energy flow back into the battery, which also requires low-impedance power transmission along the energy flow path from the foot to the battery. A low-impedance power transmission path will also benefit power generation efficiency.

C. Principle 3:Low-Impedance Mechanical Transmission

Employing gears significantly reduces the torque demands on the motors while increasing torque density. However, the addition of gearing adds reflected inertia and reflected damping of the actuator to the output shaft, and the values are multiplied by the square of the gear ratio. The increased mechanical impedance prevents the achievement of highly dynamic proprioceptive force control [21], and increases friction losses, which compromise the efficiency of energy regeneration during negative work.

However, it is difficult to generalize the optimization of the gear ratio for maximum energy efficiency. Employment of the gear transmission increases gear friction, actuator mass, and leg impedance, but also reduces E_j by increasing the overall torque density. Such a design tradeoff in a machine that has a constant angular speed can be easily characterized, but in legged locomotion, the characterization is much more involved, because legged locomotion requires highly dynamic interactions with the ground, and the transmission impedance will play a significant role in the overall dynamics of the robot. For example, increasing the gear ratio will reduce the Joule heating but it will cause higher leg impedance and increase the impact loss. More importantly, it may limit the control of the robot dynamics. Moreover, such intricacy in this tradeoff is highly variable depending on torque-speed trajectories of each joint, which are also a function of the speed of running, gait type, the scale of the robot, and so on.

Gears introduce another complexity of asymmetric friction loss, in which friction loss in the torque amplification direction is smaller than when energy flows back toward the motor [22]. This effect in spur gears has not been fully investigated; the verification of full-gear model specifically for this directional effect is ongoing work in the MIT Biomimetic Robotics Lab [23]. A full-gear interaction model is imperative for the simultaneous optimization of the actuator and gear selection to minimize losses.

For these reasons, in this paper, we propose to decouple the Joule heating from the transmission design. We provide guidelines to minimize the transmission impedance in order to maximize both the transmission efficiency and the impedance control capability. We will investigate the more accurate quantitative optimization method in future design iterations that will consider the torque trajectory data from the current robot.

D. Principle 4:Low Inertia Leg

As we often find slender legs on many biological runners, employing low leg inertia is critical for high-speed running. Low leg inertia can reduce the torque requirements during the swing phase especially during protraction phase, which involves high acceleration, and thus, high torque. Given torque limit, low inertia leg allows faster swing motion and shorter swing phase duration. A shorter swing phase duration permits a larger duty factor, the percent of stance phase of the total cycle, in a given running speed [24]. According to the vertical momentum conservation, given running speed, shorter swing time allows to reduce the required vertical momentum at each stride because a shorter swing duration yields shorter running cycle duration and reduces vertical momentum lost by gravity per stride in a steady-state running. Therefore, a large duty factor permits that the leg can stay on ground relatively longer portion and, thus, can reduce peak ground reaction force. Lower ground reaction force can lead to a lower energy consumption due to lower torque from the motors. In addition, light legs loose less energy

at touch down at every step. The amount of energy dissipated when the legs collide with the ground can be reduces with low inertia leg design.

The leg impact losses account for a significant amount of the energy loss in a running robot. Inelastic impact loss for simple linear motion is given in (1), where Δp is the impulse from impact, v^+ and v^- are the velocities of before and after impact, respectively, and m is the impact mass. A more detailed model for jointed robots can be found in [25]

$$\begin{aligned} mv^+ &= mv^- + \Delta p \\ E_i &= -\Delta E = -\frac{m}{2}[(v^+)^2 - (v^-)^2]. \end{aligned} \tag{1}$$

The aforementioned equation suggests two ways to mitigate impact losses: by minimizing the change in velocity at impact, and by reducing the impact mass. As the impact velocity is related to the robot's relative velocity, one approach to reducing impact losses is to control the retraction speed of the leg before impact on the ground [26]. Another way to decrease impact losses is to reduce the impact mass. A lower distal mass is desirable for minimizing impact and also reduces the energy required to cycle the legs.

These four principles were implemented in the design of the MIT Cheetah, as shown in Fig. 2. It is noted that some of these principles are coupled each other and can cause tradeoffs. For example, the low transmission ratio is favorable for minimizing the transmission loss, impact loss, and maximizing regeneration at the expends of more torque from the motor, and hence, more heat dissipation. Finding quantitatively optimal design involves a large number of parameters intertwined in a very complex problem because changes in gear ratio will change the dynamic characteristic of the actuators, which will yield different locomotion dynamics. The selection of such design parameters should be customized for the purpose of the robot. In the design of the MIT Cheetah robot, we minimize the gear ratio for force control bandwidth, which might not be the best choice for energy efficiency. However, unlike the design of inherently stable systems such as cars, the control aspect should be fully addressed as well as energy efficiency. Detailed implementation is explained in Section III.

III. Implementation of Design Principles on the MIT Cheetah Robot

A. Large Gap Radius Motor

While holding the motor mass constant, the torque density of the motor can be improved by increasing the gap radius: the radius of the gap between the motor stator windings and the permanent magnets on the rotor. Seok *et al.* [21] has shown that the gap radius is a principal measure of the motor performance. The analysis is performed with the assumptions that the rotor and stator maintain constant radial thickness, the mass m stay constant, and that the average shear stress applied to the rotor stays constant (see Fig. 5). The torque density scales by approximately $\tau/m \propto r_{\text{gap}}$, the torque per inertia scales by $\tau/J \propto r_{\text{gap}}^{-2}$, and the torque squared per electric power, also known as motor constant square, a measure of torque production efficiency, scales

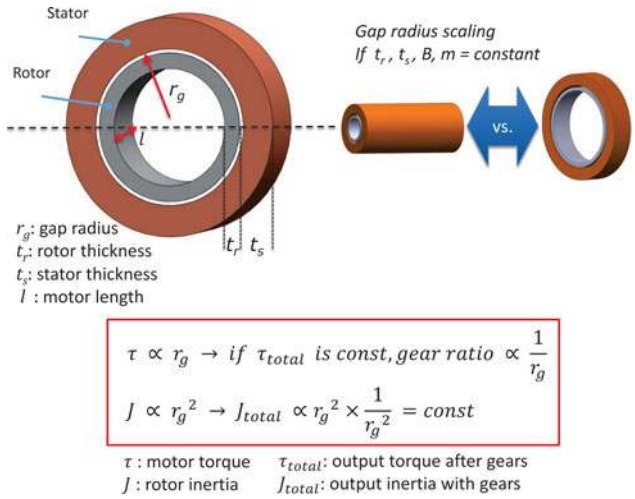

Fig. 5. Gap radius scaling of electromagnetic motor with a constant mass.

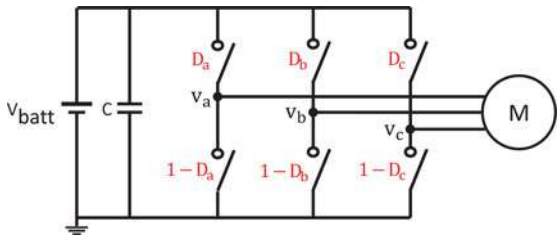

Fig. 6. Three-phase motor driver.

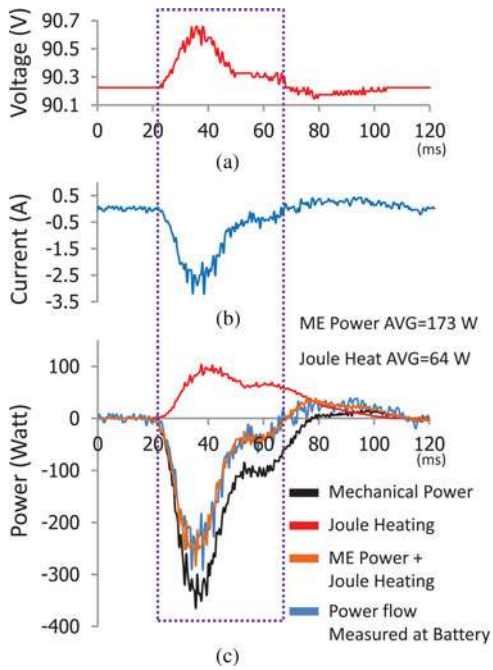

Fig. 7. (a) Voltage of the battery supply line during the regeneration experiment. (b) Current flowing out of the batteries during the regeneration experiment. (c) Mechanical power, Joule heating dissipation, and battery power measured during the experiment. Note that 63% of the negative mechanical work done by the motors is recovered by the batteries in the experiment.

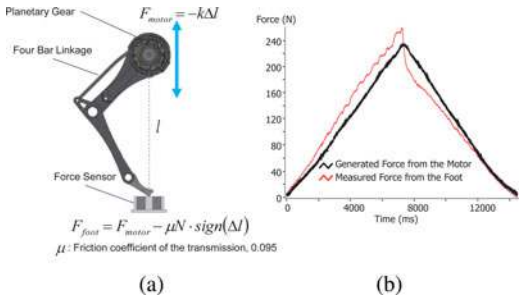

Fig. 8. (a) Experimental setup used for determining loss in the mechanical transmission. The force at the foot is calculated using the torques applied by the motors and compared against a force sensor under the foot. (b) Experimental data showing the difference between the expected force on the foot as generated from the motors, and the actual force measured.

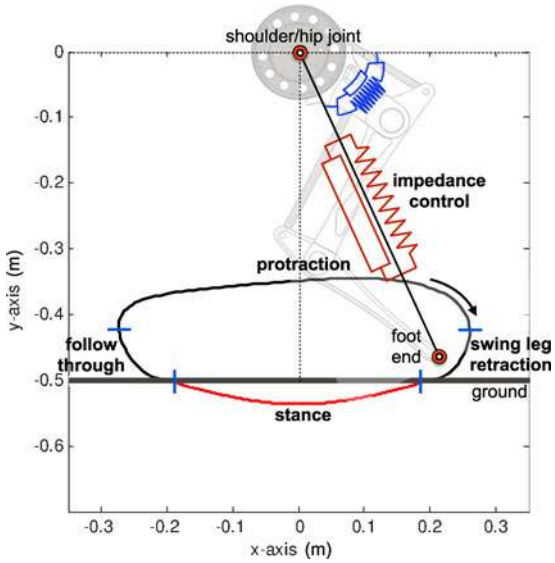

Fig. 9. Desired swing phase (black solid line) and stance phase (red solid line) trajectory for the front leg, as well as the desired ground position (straight black solid line at -0.5 m). The point $(0, 0)$ is the location of shoulder/hip of the robot.

by $\tau^2/I^2R = K_M^2 \propto r_{\text{gap}}^3$. Therefore, in a design space where the motor mass and the continuous torque requirement are held constant while the gap radius is free to vary and the massless and frictionless gear train are added to meet the torque requirement, the output torque, and total reflected inertia are independent of the gap radius and corresponding gear ratio. This result indicates that if the analysis includes gear inertia, gear friction, as the gap radius of the motor increases, the results will favor the motor with the larger gap radius because it will have a smaller gear ratio and fewer gear-train stages; this results in less friction loss, higher torque density, and higher bandwidth. Therefore, in this particular design space, there is no tradeoff.

Using this insight, a custom three-phase synchronous motor is designed as shown in Fig. 18, which is optimized for peak torque density for high-speed running [27] (gap radius: 48.5 mm, torque constant: 0.4 Nm/A, motor constant: 0.64 Nm/$\sqrt{\text{W}}$, weight: 1 kg, phase resistance: 0.26 Ω, peak torque: 30 Nm [3]).

[3]extrapolated from demagnetization current.

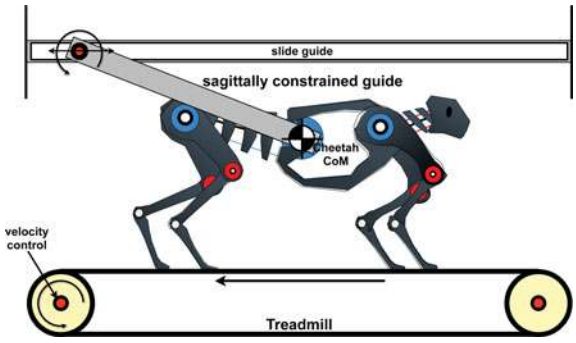

Fig. 10. Experimental setup of MIT Cheetah on treadmill. Motion is constrained to the sagittal plane.

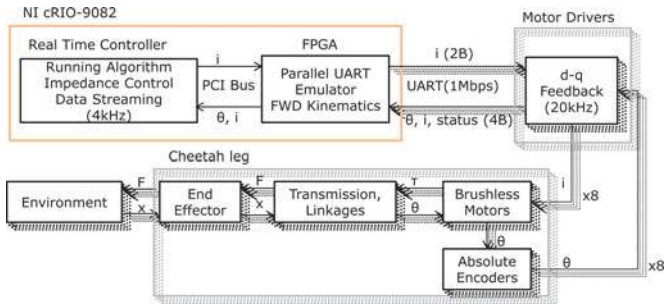

Fig. 11. Control system diagram for the MIT Cheetah Robot. The main controller (NI cRIO-9082) has the real-time multicore controller and the FPGA and controls eight BLDC motor drivers in parallel.

Fig. 12. High-speed video captured at 500 fps depicting 150 ms of the MIT Cheetah running at 6 m/s

The continuous torque density of this motor is also about 1.5 times compared with the commercial motor currently used in the MIT Cheetah (Emoteq HT-5001, gap radius: 38.5 mm, torque constant of 0.27 Nm/A, motor constant: 0.43 Nm/$\sqrt{\text{W}}$, weight: 1.3 kg, phase resistance: 0.354 Ω, and peak torque: 10 Nm). The Emoteq motor is used for all of the experiments shown in this paper.

B. Motor Drive Electronics Design for Regeneration

In order to realize efficient bidirectional energy flow, we employ proprioceptive force-control actuators [21]. This approach allows programmable leg impedances and high bandwidth control of large forces in a simple structure without series compliance or force sensors.

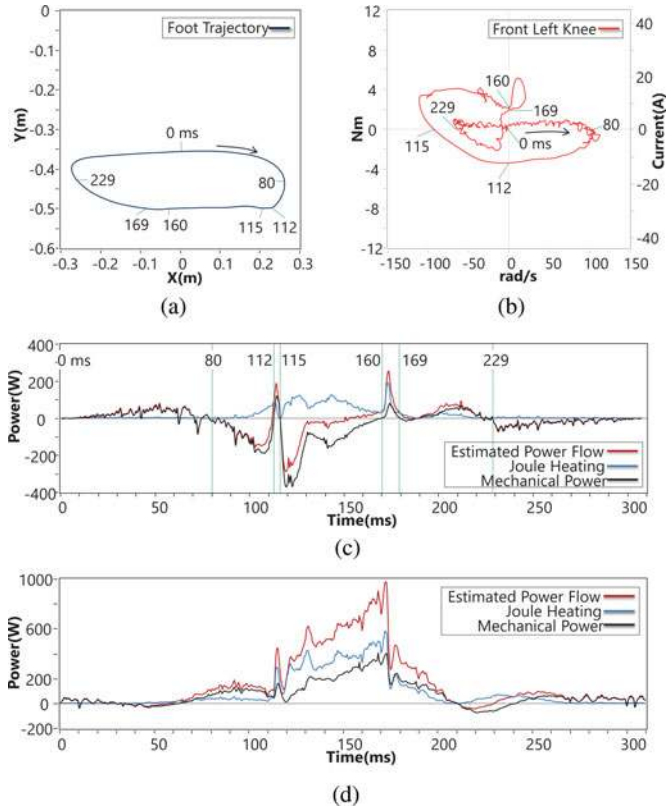

Fig. 13. Plots of data at 6 m/s trot running. (a) shows the measured trajectory of the front left foot. The direction of the trajectory is clockwise. One period of the trajectory is 310 ms and the major times are written on the plot. (b) shows the angular velocity versus torque of the front left knee motor. The top-right and the bottom-left quadrants represent positive power, and the top-left and the bottom-right quadrants represent negative power. (c) shows the power consumptions of the front left knee motor. The black line represents mechanical power, and the blue line represents Joule heating. The red line represents estimated power flow from the motor. The positive value of the red line means power flows from the batteries to the motor, and the negative value means power flows from the motor to the batteries. (d) shows the power consumptions of the front left hip motor.

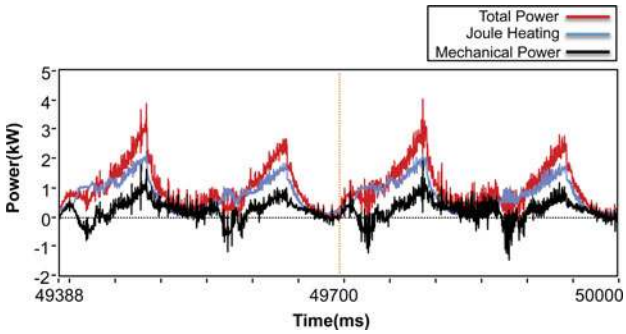

Fig. 14. Power consumption of all motors during 6 m/s trotting. The blue line is the sum of powers used as Joule heating of all motors. The black line is the sum of mechanical powers of all motors. The red line represents the total power consumption, which is the sum of Joule heating and mechanical power.

In order to allow for energy regeneration in electromagnetic conversion, the architecture of the motor driver on the MIT Cheetah is designed to act like a three-phase generator when motors perform negative work [28], [29]. Specifically, the motor driver is a custom switching converter built from three FET half bridges, capable of driving a three-phase motor at 60 A from a 100-V supply. The topology is shown in Fig. 6. Using the direct quadrature zero transformation, the driver commands the phase voltages of the motor to control the torque producing q-axis current while controlling the d-axis current to zero. When energizing the motor, the motor driver bucks down the battery supply voltage to the desired phase voltages. In regenerative braking mode, the driver controls the q-axis currents to flow back into the driver and charge the batteries.

The motor driver developed for the MIT Cheetah robot commands voltages to each motor lead using pulse-width modulation. Here, we designate the duty cycle of a single phase as D and the applied motor voltage as Dv_{batt}. In the backward power flow direction, the motor driver acts a boost converter and the stepped-up voltage is $\frac{1}{1-D}v_{\mathrm{bemf}}$, where v_{bemf} is the back-EMF produced at the motor phase. If $\frac{1}{1-D}v_{\mathrm{bemf}} > v_{\mathrm{batt}}$, then the energy from braking the motor recharges the batteries.

The drive electronics were tested for conversion efficiency with the Emoteq motor and Joule heating from the torque producing q-axis current was found to be dominant. FET switching loss is on average 3.1 W. The FET phase resistance including the resistance due to the traces on the PCB is 0.0047 Ω, which is on the order of 1% of the motor phase resistance. Measurements of the current in the motor gave an RMS d-axis current that was 4% of the q-axis current. Therefore, the dissipated power from the d-axis current is 0.16% of the total power, and the power consumption by Joule heating can be approximated as $P_j = (I_q^2 + I_d^2)R \approx I_q^2 R$.

To verify the effective regeneration during negative work, a simple experiment was performed. The MIT Cheetah robot was commanded to hold a fixed position with one leg held by a virtual spring with proportional gain of 5 kN/m and virtual damping of 100 Ns/m. Then, to simulate the impact that occurs during running, the robot was lifted and dropped onto the one leg being commanded to hold a constant position. The data from the experiment, shown in Fig. 7, confirm that the batteries were indeed recharged. The voltage of the battery line shown in Fig. 7(a) experienced a voltage spike from the boosted motor voltage and Fig. 7(b) clearly shows current flow back into the battery. Fig. 7(c) accounts for the mechanical work done by the motor, the amount of the Joule heating in the motor windings and the power consumption at the batteries. 63% of the negative mechanical work done by the motors was recovered by the batteries in the experiment. The charging efficiency of lithium polymer batteries can be over 95% [30], showing that most of the regenerated energy goes into recharging the batteries. However, in most steady-state running cases, the regenerated energy from one motor is fed to other motors. This is shown in the data in Fig. 14; there is a brief moment when the total power from the battery is zero, but not negative.

C. Low Gear Ratio Transmission

To minimize the losses associated with cascading gear loss, the number of gear stages is restricted to only one stage in each motor. A single gear stage in a commercial gearbox can

lose approximately 10% of the input power [31]. This value is dependent on the gear quality and detailed parameters of gear, such as module, pressure angle, and so on. In general, a higher gear ratio will have a higher friction loss, but increasing the number of gear train stages significantly increases friction, overall inertia of the gears, backlash, and complexity of the structure. For example, it is more desirable to have a higher gear ratio in one stage than to split it into two stages. Thus, the MIT Cheetah robot uses a custom designed single stage of planetary gearing with a gear ratio of 5.8:1 on each motor, the largest ratio that can be obtained at a single stage in the given space. The relatively low ratio reduces the contribution of reflected actuator dynamics on the impedance of the transmission output. However, this gear ratio is not optimized due to the lack of a detailed loss model.

The friction of the mechanical transmission needs to be measured to determine its effect on proprioceptive control [21]. A diagram of the experimental setup is shown in Fig. 8(a). The leg was subjected to a compression and decompression cycle applied externally by a linear material testing device. The motors were commanded to act as a virtual spring to the resist the compressive force of the machine. We measured the expected output force from the motor current and compared it to the force at the foot as measured by a commercial force sensor. The two forces are shown in Fig. 8(b), and the transmission loss is modeled as a force-dependent coulomb loss acting against the direction of travel. The resulting friction coefficient is 0.095, equivalent to 9.5% power loss.

D. Biotensegrity Leg

As a part of the effort to minimize leg inertia, we implemented a bioinspired leg design approach in the MIT Cheetah, namely, a tendon-bone colocation architecture [32]. We hypothesized that the bones of the animals legs carry mostly compressive loads, while the muscles, tendons, and ligaments carry the tensile loads [33]. This distribution makes effective use of the relative advantages of each biological material to achieve a lightweight yet strong structure. To achieve this same tendon-bone colocation architecture, a tendon was integrated into the design of the MIT Cheetah leg, linking the foot to the knee. Experiments show that this architecture reduces the stress experienced by the bone during stride by up to 59%. A composite bone-like structure of the robot leg was fabricated drawing inspirations from biological structures. A rigid and light polyurethane foam core for the leg was covered in a high stiffness polyurethane resin to form a composite with high strength but low inertia. Further details on the tendon-bone colocation design architecture and experiments performed on the robot leg can be found in [32].

E. Dual Coaxial Motor Design

Observations of biological running animals such as horses show that most of the musculature in the legs is concentrated proximal to the shoulder of the animal. Based on the inspiration from this observation, the architecture of the leg of the MIT Cheetah is specifically designed to minimize inertia. Two motors are placed coaxially in the shoulder: one motor actuates the shoulder joint, while the other actuates the knee through the use of a four-bar steel linkage. The rotational motions of the two coaxial motors are independent. One is coupled to the shoulder joint, while the other motor is coupled to the knee joint. The center of mass is 45 mm from the center of rotation [21]. This architecture is in contrast to the traditional serial link architecture shown in many humanoid robot arms, where the actuators are located at every joint, increasing the inertia of the distal links, which is not conducive to high-speed running. Such architecture also benefit in proprioceptive force control by minimizing inertial forces of the legs under high acceleration. The architecture of Phantom was designed using a similar principle [34].

IV. Experiment

This section shows the experimental results of a test of the trotting gait of the MIT Cheetah. The current running speed is up to 6 m/s (13.5 mph) and mechanically constrained to stay in the sagittal plane. The robot is powered by an external battery pack and a dummy weight simulating the battery mass is placed on the robot. The next section briefly explains the running algorithm, the Section IV-B explains the experimental setup, and the Section IV-C discusses the results of the running experiments.

A. Control Algorithm

A new control algorithm for high-speed quadrupedal locomotion has been developed for the MIT Cheetah. This algorithm hierarchically consists of a gait pattern modulator, a gait trajectory generator, and an leg impedance controller. The swing foot trajectory is designed by using a 12 points Bézier curve and the stance foot trajectory is designed by a magnitude-tunable sine wave for the experiment as shown in Fig. 9.

The operator can determine the desired speed v_d and phase differences for all legs in one stride period. The pattern modulator can describe various animal gait patterns by synchronizing individual legs to a specific pattern with a target speed; For the trot gait, the diagonal legs and the off-diagonal legs has the opposite phases. Then, the gait pattern generator generates four signals for each leg with the desired phase differences. Subsequently, the gait trajectory generator maps these pattern signals to the designed gait trajectories for each legs. The designed trajectory consists of two parts: swing phase and stance phase. We fixed the desired swing time as 250 ms, and decreased the desired stance time from 850 to 60 ms for increased speed by

$$v_d = \frac{2L_{\mathrm{span}}}{T_{st}} \tag{2}$$

where L_{span} is the half of the stride length. Each foot was controlled by the impedance controller, and the virtual impedance gains commanded by the controller are listed in Table I. These particular values were chosen by hand tuning and the virtual damping gain was maximized up to the stable limit of the system. Therefore, the designed gait trajectories at each leg act as the equilibrium points of the leg impedance controller at each instant. The chosen gait pattern was triggered when the left front

TABLE I
IMPEDANCE GAIN VALUES FOR THE EXPERIMENT

	Description	Value
$K_{p,r}$	Virtual radial stiffness	5000 N/m
$K_{d,r}$	Virtual radial damping	100 Ns/m
$K_{p,\theta}$	Virtual angular stiffness	100 Nm/rad
$K_{d,\theta}$	Virtual angular damping	4 Nms/rad

foot of the robot touched the ground and generated one stride. This process was repeated while the robot was running, and it successfully modulated the gait pattern over different speeds. This algorithm allows for stable trot running up to the limit of the treadmill speed (6 m/s).

B. Experimental Setup

An experimental setup was constructed to facilitate the testing of the MIT Cheetah running. A figure representing the experimental setup can be seen in Fig. 10. The MIT Cheetah runs on the commercial fitness treadmill (SOLE TT8) that has been modified to be 3.5-m long to accommodate the length of the robot. The maximum speed of the treadmill is 6 m/s, which limits the test speed of the running robot.

A linear guide rail system is mounted above the treadmill. This configuration ensures that the motions of the MIT Cheetah are constrained within the sagittal plane without any roll and yaw, but the robot is free to move in both vertical and fore-aft translation and to rotate along the pitch axis. For safety, the batteries were not located on the robot, but a 3-kg dummy mass was added to the cheetah body to simulate the battery weight.

The robot control system is comprised of four layers of controllers: the motor drivers, the parallel UART emulators, the real-time multicore controller, and the monitoring PC. Each motor driver (MCU: Microchip dsPIC30F6010) handles the current control of one BLDC motor at 20 kHz. The NI cRIO-9082 houses both the parallel UART emulators and the real-time multicontroller, and all the software is programmed by NI LabVIEW. Control hardware is shown in Fig. 4, and the system diagram is shown in Fig. 11.

C. Experimental Results

We measured the voltage and the current data of each motor and the treadmill speed. The estimated speed from the robot and the treadmill speed has a 0.15-m/s bounded error, so the estimated data are used for the following analysis. High-speed video is captured at 500 fps by a high-speed camera (Mikrotron MC1363) with the NI PCIe-1429 frame grabber. Captured running images can be seen in Fig. 12

Fig. 13 shows the data at 6 m/s. Fig. 13(a) is the measured trajectory of the front left foot with the same coordinates as in Fig. 9. The direction of the trajectory is clockwise. One period of the trajectory is 310 ms and the major times are written on the plot. Fig. 13(b) shows the angular velocity versus torque of the front left knee motor. The top-right and the bottom-left quadrants represent positive power, and the top-left and the bottom-right quadrants represent negative power. Fig. 13(c) and (d) shows the power consumptions of the front left knee motor and front left hip motor, respectively, for one cycle. The black line represents mechanical power, and the blue line represents Joule heating. The red line represents estimated power flow from the motor. The positive value of the red line means power flows from the batteries to the motor, and the negative value means power flows from the motor to the batteries.

$$\begin{aligned}\text{Mechanical power} &= \sum_{8\text{motors}} \tau \times \omega \\ &= \sum_{8\text{motors}} K_t \times I_q \times \omega \\ \text{Joule heating power} &= \sum_{8\text{motors}} I_q^2 R,\ I_d = 0 \\ \text{Total power} &= \text{Mechanical power} \\ &\quad + \text{Joule heating power.} \end{aligned} \tag{3}$$

Mechanical power, Joule heating, and total power were calculated using the aforementioned equation. The previous research [1] and Fig. 7(c) proved that power consumption measured at battery matches up with the sum of mechanical power and Joule heating, so this calculation is used for power-flow estimation from a motor. The power consumption by the other electronics is included in Joule heating.

The regenerated work to negative work ratio is 61% during one cycle in Fig. 13(c). The total mechanical work for one cycle is -8310 J, where positive work is 3470 J and negative work is -11780 J. Regenerated work from negative work is -7163 J. The hip motor did mostly positive work, while the knee motor experienced phases of significant negative work. The major regeneration happened between 80–112 ms and 115–160 ms, where the knee motor torque rapidly decelerated the opening speed of the knee joint and the when leg was under the stance phase where the leg pushed the ground but the actual leg length became shorter. This shows that electrical regeneration is an effective alternative solution to mechanical springs for storing energy.

Fig. 14 is the plot of the power consumption of all motors during 6 m/s trotting. It can be seen that the mechanical power (black line) showed negative values, which were regenerated during locomotion. This regenerated power was supposed to charge the battery or be consumed in the other legs. The total power briefly reached zero but did not go negative, which means that the generated energy when a pair of legs do negative work was fed to the other pair of legs to do positive work even though significant energy regeneration happened in the knee motors, as shown in the Fig. 13(c). In most gaits, we expect that most regenerated energy goes to other joint actuators and that little energy recharges the batteries. However, in several exceptional cases, such as during the ground phase in a pronk gait or landing from jumping, we expect that a significant amount of energy will recharge the batteries.

One of the most remarkable results in this experiment is that Joule heating, which results in 76% of total power, is by far the predominant mode of the power consumption. Table II shows

TABLE II
MIT CHEETAH POWER CONSUMPTION VALUES DURING 6 M/S RUNNING

				With 3 kg Battery (465 Wh)	
Total Power	Joule Heating	Mechanical Power	COT	Running Time	Distance
973 W	739 (76%)	234 (24%)	0.5	0.48 h	10.3 km

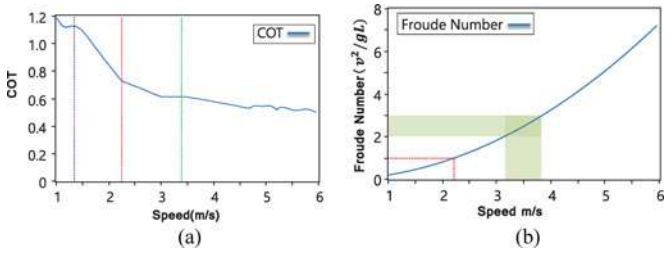

Fig. 15. Plot shows TCoT and Froude number with respect to running speed from 1 to 6 m/s. (a) Red line indicates the start of running (2.3 m/s). The green line shows when the swing leg retraction speed reaches 3.4 m/s. (b) Red line represents a Froude number of 1.0, where animals switch from walk to run. For the MIT Cheetah robot, the Froude number of 1 corresponds to 2.3 m/s, the speed at which the robot switches from walk to run. The green area is the region of Froude numbers between 2.0 and 3.0, where quadrupeds change the gait from trot to gallop.

several attributes of the average power consumption at 6 m/s. Of the 973 W consumed, 739 W is lost in Joule heating, while 234 W is consumed by the net mechanical work, which is dissipated through gear friction, joint friction, and interaction loss. From this data, we can predict that the MIT Cheetah robot can run 10.3 km with 3 kg (465 Wh) LiPo Battery. The large contribution of the Joule heating loss can be mitigated by increasing the gear ratio. Future designs will need to compare the efficiency gains in Joule heating to the tradeoff in transmission dissipation by optimizing the gear ratio. Design issues that may arise from more gearing include additional complexity and mass of the mechanisms, as well as increased reflected inertia, which contributes to higher impact loss, and poorer impedance control.

The MIT Cheetah weighs 33 kg and the TCoT is 0.5, which is similar to that of other biological runners of similar mass. Fig. 1 shows the TCoT of animals in nature as well as man-made vehicles. The TCoT of representative robots are overlaid [4] to compare the metabolic energy consumption of animals with the overall power consumption of mobile robots. For animal data, the three classes of locomotion (runners, fliers, and swimmers) occupy distinct regions of the plot of TCoT versus body mass. As seen in the graph, the MIT Cheetah robot is right below the runners' line, which means its energy efficiency is similar to that of a biological runner of similar mass.

We observed an interesting trend in Fig. 15(a) that shows the change in TCoT as the MIT Cheetah accelerates from 1 to 6 m/s in a trot. So far, no biological runners of a similar scale have been observed to trot up to this speed, possibly because the trot is energetically much more expensive than other gaits such

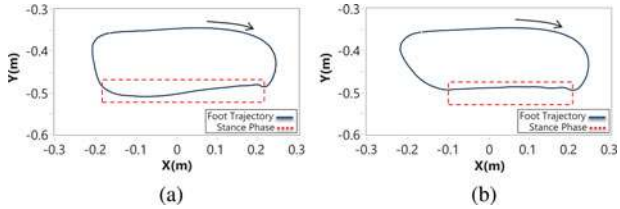

Fig. 16. Plots show measured foot trajectory with the same coordination in Fig. 9. The blue line represents the measured foot trajectory, and the red dotted box represents the stance phase. (a) Plot is one cycle trajectory at 1.4 m/s, where the duty factor is 0.5. (b) Plot is at 2.3 m/s, where the shoulder height from the ground starts reaching its lowest point near midstance.

as canter or gallop. The Froude numbers[4] between 2.0 and 3.0 is the region where the second transition happens from trot to canter or gallop [35]. The energetic cost data in horses show that horses have a preferred speed for trot and if their trot speed deviates from that speed, the TCoT increases and they switch to another gait if it is more efficient. Interestingly, the TCoT of the MIT Cheetah decreases continuously up to 6 m/s. The TCoT may increase after a certain higher speed but this phenomenon is not yet examined in this test. For this particular controller, the robot's preferred speed of trot is higher than 6 m/s. Such high-speed trotting requires a high stride frequency and high-speed leg motion, which are usually not desirable in animals. The major reason that explains this result might be the characteristic difference between electromagnetic motors and biological muscle. For example, muscles have a distinct force–displacement and a force–velocity constraints described by Hill's model [36], but torque of electric motors is independent from its position and velocity, assuming that we have an electric source whose voltage is high enough.

During the period when the duty factor (the fraction of a stride during which a given foot is on the ground) goes under 0.5 (from 1 m/s to 1.4 m/s), the TCoT drops and becomes stationary. From 1.4 m/s to 2.3 m/s, the TCoT drops rapidly. At 2.3 m/s, the MIT Cheetah starts running[5] as shown in Fig. 16 and this corresponds to a less steep decrease in TCoT. At 3.4 m/s the swing leg retraction speed is increased to match the ground speed, and the TCoT remains stationary at the region around the speed of 3.4 m/s. The minimum TCoT reached is 0.5025 at 5.95 m/s.

At 2.3 m/s, which corresponds to a Froude number of 1, the gait typically changes to running, as shown in Figs. 15(b) and 16(b). When the Froude number is around 1.0, the centrifugal force equals to gravitational force, and most animals switch from walking gaits to running gaits [35], and the same transition is shown in the Cheetah robot.

Although the MIT Cheetah's running gait is not optimized for efficiency, it shows an exceptional mechanical cost of transport

[4]The Froude number is the ratio of the centripetal force around the center of motion, the foot, and the weight of the animal/robot. It can be calculated by v^2/gl, where v is the velocity, g is the acceleration due to gravity, and l is the characteristic length of the leg.

[5]Here, we follow McMahon and McGeer's definition of running [37], [38]. In running, midstance is the instant of minimum height, in other words, the center of mass reaches its lowest point near midstance.

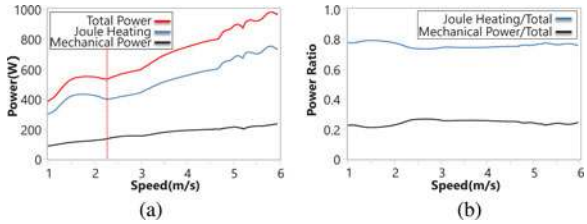

Fig. 17. Plot shows Joule heating and mechanical power, and the ratios between them with respect to running speed from 1 to 6 m/s. (a) Red line represents the total power consumption from the battery, which is the sum of Joule heating and mechanical power. The blue line is the power used in Joule heating. The black line is the mechanical power. (b) Blue line is the ratio of Joule heating to the total power, and the black line is the ratio of mechanical power to the total power. The ratios are not changed significantly with respect to speeds.

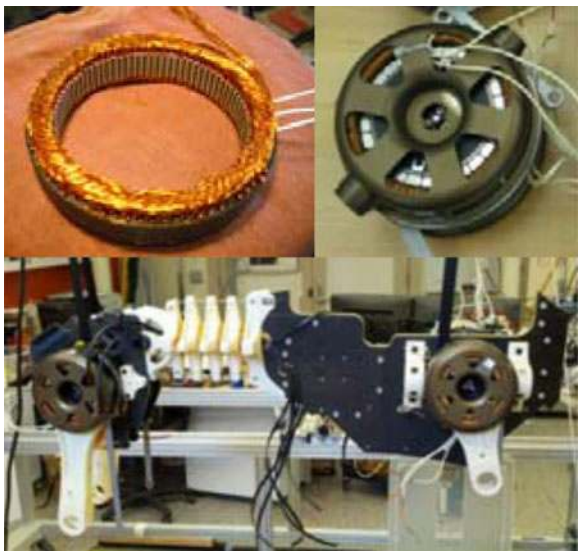

Fig. 18. Newly developed MIT motor and MIT Cheetah v.2.

(MCoT). MCoT is calculated based on mechanical work instead of total power consumption; note that the mechanical work only counts total positive work and doesn't substrate out the negative work [17]. Researchers who have an interest in optimizing the gait pattern and trajectory for efficiency tend to use MCoT for showing the performance of their robots. The MIT Cheetah has MCoT of 0.12 at 6 m/s, which is 4 times better than the Scout II (MCoT 0.47) [15], around 13 times better than the Honda ASIMO (MCoT 1.6) [39], and its performance is similar to that of the energy-optimized robot MABEL (MCoT 0.14), which has an external power source and a real-time controller [39], whereas the MIT Cheetah has everything inside. Moreover, it exceeds the efficiency of animals of similar weight, such as dogs and goats (MCoT 0.2 at 2.85 m/s trot) [40].

However, as discussed in Section I it is critical for robot designers to consider the TCoT, including not only mechanical power but also other dissipative energy losses such as Joule heating. Fig. 17 shows the change in power consumption as the MIT Cheetah accelerates from 1 to 6 m/s in a trot gait. It can be seen that Joule heating accounts for roughly 75% of the energy consumption from the battery over the whole range of speed. The

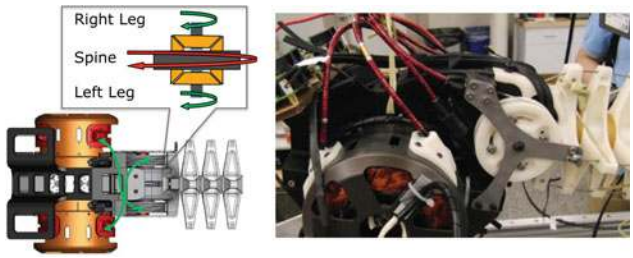

Fig. 19. Spine Differential Cabling. As the MIT Cheetah runs, the steel cables couple the motions of the rear legs to the motions of the spine in the sagittal plane. The green color arrows indicate how the cabling couples each leg to the differential input shafts, which then drive the center drum to actuate the spine.

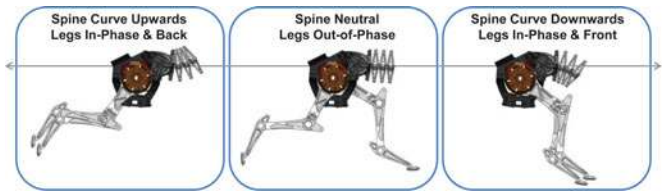

Fig. 20. Differential spine actuation. During high-speed running, the spine can be actuated by choosing to actuate the rear legs either in-phase or out-of-phase. When the legs are in-phase and backward, the differential coupling would cause the spine to arch upwards, increasing the stride length of the MIT Cheetah. When the legs are in-phase and forward, the differential would make the spine curve downwards, tucking the rear legs further forward. Otherwise, when the legs are out-of-phase, the spine remains neutral.

ratio of the mechanical power to the total power consumption is only about 25%, which is independent from energy loss from the actuators and highly depends on the control algorithms. These data suggest that for any legged robots, the design of the motor is critical to increasing efficiency. Specifically, use of high torque-density motors, as described in Section II-A, is directly related to this goal of minimizing heat dissipation.

V. Conclusion and Future Work

Based on the energy flow of a locomotive system, four major design principles were highlighted and successfully implemented to the MIT Cheetah. The principles include high torque-density motors, an energy regenerative electronic system, low loss transmission, and low leg inertia. The MIT Cheetah achieved a cost of transport of 0.5 that rivals running animals and is significantly lower than other running robots.

A feature that will be used in future experiments is the switchable differentially actuated spine that can select between rigid, passive, and actuated modes. It is composed of vertebrae elements that are separated by polyurethane rubber rings, which can store elastic energy during spine flexion. The design does not require an additional actuator and instead uses a differential to couple the spine motion to the rear legs as shown in Fig. 19. Fig. 20 shows the motion of the of the spine in the actuated mode. By selecting between the different modes of the spine, the effect of spine dynamics on running efficiency can be explored.

From the experimental results, specifically analysis of energy loss in the components of the system, we learned that Joule

heating is the major power loss during locomotion. In order to reduce the Joule heating from electric motor, we have developed a new custom-designed three-phase motor, shown in Fig. 18 focused on reducing heat loss and maximizing torque density. The preliminary experiment data show that it has three times the saturation (peak) torque, 1.5 times the torque constant, and 0.73 times the phase resistance of the current motor. The motors are designed to be a drop-in replacement and when they are implemented on the MIT Cheetah robot, it is expected that the TCoT will be reduced to 0.25, which is superior to efficiency of biological runners and similar to that of fliers in nature.

ACKNOWLEDGMENT

The authors would like to thank V. Tucker, Prof. Emeritus at Duke University for his early investigation of animal locomotion that have inspired modern robots to strive toward the efficiencies found in nature, and National Instruments for hardware support.

REFERENCES

[1] S. Seok, A. Wang, Chuah, M. Y. (Michael), D. Otten, J. Lang, and S. Kim, "Design principles for highly efficient quadrupeds and implementation on the MIT cheetah robot," in *Proc. IEEE Int. Conf. Robot. Autom.*, 2013, pp. 3307–3312.

[2] P. Bhounsule, J. Cortell, and A. Ruina, "Design and control of ranger: An energy-efficient, dynamic walking robot," in *Proc. 15th Int. Conf. Climbing Walking Robots Support Technol. Mobile Mach.*, Jul. 2012, pp. 441–448.

[3] V. A. Tucker, "The energetic cost of moving about: Walking and running are extremely inefficient forms of locomotion. Much greater efficiency is achieved by birds, fish and bicyclists," *Amer. Scientist*, vol. 63, no. 4, pp. 413–419, 1975.

[4] A. Ruina. (2012, Sep.). Cornell ranger 2011, 4-legged bipedal robot. [Online]. Available: http://ruina.tam.cornell.edu/research/topics/ locomotion_and_robotics/ranger/Ranger2011/

[5] O. Auro and P. Komi, "The mechanical efficiency of pure positive and pure negative work with special reference to the work intensity," *Int. J. Sports Med.*, vol. 7, pp. 44–49, 1986.

[6] R. Tedrake, T. Zhang, M. Fong, and H. Seung, "Actuating a simple 3D passive dynamic walker," in *Proc. IEEE Int. Conf. Robot. Autom.*, Apr. 2004, vol. 5, pp. 4656–4661.

[7] J. Hurst, J. Chestnutt, and A. Rizzi, "The actuator with mechanically adjustable series compliance," *IEEE Trans. Robot.*, vol. 26, no. 4, pp. 597–606, Aug. 2010.

[8] M. Hutter, C. Gehring, M. Bloesch, M. Hoepflinger, C. D. Remy, and R. Siegwart, "Starleth: A compliant quadrupedal robot for fast, efficient, and versatile locomotion," presented at the *Int. Conf. Climbing and Walking Robots*, Baltimore, MD, USA, 2012.

[9] S. Kim, J. Clark, and M. Cutkosky, "iSprawl: Design and tuning for high-speed autonomous open-loop running," *Int. J. Robot. Res.*, vol. 25, no. 9, pp. 903–912, 2006.

[10] S. Wolf and G. Hirzinger, "A new variable stiffness design: Matching requirements of the next robot generation," in *Proc. IEEE Int. Conf. Robot. Autom.*, May 2008, pp. 1741–1746.

[11] G. Folkertsma, S. Kim, and S. Stramigioli, "Parallel stiffness in a bounding quadruped with flexible spine," in *Proc. IEEE/RSJ Int. Conf. Intell. Robots Syst.*, Oct. 2012, pp. 2210–2215.

[12] F. Iida, G. Gomez, and R. Pfeifer, "Exploiting body dynamics for controlling a running quadruped robot," in *Int. Conf. Adv. Robot.*, Jul. 2005, pp. 229–235.

[13] T. Takuma, M. Ikeda, and T. Masuda, "Facilitating multi-modal locomotion in a quadruped robot utilizing passive oscillation of the spine structure," in *Proc. IEEE/RSJ Int. Conf. Intell. Robots Syst.*, Oct. 2010, pp. 4940–4945.

[14] Q. Zhao, K. Nakajima, H. Sumioka, X. Yu, and R. Pfeifer, "Embodiment enables the spinal engine in quadruped robot locomotion," in *Proc. IEEE/RSJ Int. Conf. Intell. Robots Syst.*, Oct. 2012, pp. 2449–2456.

[15] I. Poulakakis, J. A. Smith, and M. Buehler, "Modeling and experiments of untethered quadrupedal running with a bounding gait: The Scout II robot," *Int. J. Robot. Res.*, vol. 24, no. 4, pp. 239–256, 2005.

[16] D. Campbell and M. Buehler, *Preliminary Bounding Experiments in a Dynamic Hexapod*. New York, NY, USA: Springer, 2003.

[17] P. Bhounsule, J. Cortell, B. Hendriksen, J. Karssen, C. Paul, and A. Ruina, *Int. J. Robust. Res.*, vol. 33, pp. 1-17, 2014.

[18] D. Renjewski, A. Spröwitz, and J. Hurst, "Atrias—A human size compliant bipedal robot walks efficiently," presented at the *Dynamic Walking Conf.*, Pittsburgh, PA, USA, 2013.

[19] A. Ruina, J. Bertram, and M. Srinivasan,, "A collisional model of the energetic cost of support work qualitatively explains leg sequencing in walking and galloping, pseudo-elastic leg behavior in running and the walk-to-run transition," *J. Theoretical Biol.*, vol. 237, no. 2, pp. 170–192, 2005.

[20] M. Yoong, Y. Gan, G. Gan, C. Leong, Z. Phuan, B. Cheah, and K. Chew, "Studies of regenerative braking in electric vehicle," in *Proc. IEEE Conf. Sustainable Utilization Develop. Eng. Technol.*, Nov. 2010, pp. 40–45.

[21] S. Seok, A. Wang, D. Otten, and S. Kim, "Actuator design for high force proprioceptive control in fast legged locomotion," in *Proc. IEEE/RSJ Int. Conf. Intell. Robots Syst.*, Oct. 2012, pp. 1970–1975.

[22] M. Dohring, E. Lee, and W. Newman, "A load-dependent transmission friction model: Theory and experiments," in *Proc. IEEE Int. Conf. Robot. Autom.*, May 1993, vol. 3, pp. 430–436.

[23] A. Wang, "Directional Impedance of Geared Transmissions," Master's thesis, *Massachusetts Inst. of Technol.*, Cambridge, MA, USA, 2012.

[24] P. G. Weyand, D. B. Sternlight, M. J. Bellizzi, and S. Wright. (2000). Faster top running speeds are achieved with greater ground forces not more rapid leg movements. *J. Appl. Physiol*. [Online]. 89(5), pp. 1991–1999. Available: http://jap.physiology.org/content/89/5/1991.abstract

[25] I. Walker, "The use of kinematic redundancy in reducing impact and contact effects in manipulation," in *Proc. IEEE Int. Conf. Robot. Autom.*, May 1990, vol. 1, pp. 434–439.

[26] M. Haberland, J. Karssen, S. Kim, and M. Wisse, "The effect of swing leg retraction on running energy efficiency," in *Proc. IEEE/RSJ Int. Conf. Intell. Robots Syst.*, Sep. 2011, pp. 3957–3962.

[27] N. Farve, "Design of a low-mass high-torque brushless motor for application in quadruped robotics," Master's thesis, Massachusetts Institute of Technology, Cambridge, MA, USA, 2012.

[28] M. K. Yoong, Y. H. Gan, G. D. Gan, C. K. Leong, Z. Y. Phuan, B. K. Cheah, and K. W. Chew, "Studies of regenerative braking in electric vehicle," in *Proc. IEEE Conf. Sustainable Utilization Develop. Eng. Technol.*, 2010, pp. 40–45.

[29] D. Torres and P. Heath, "Regenerative braking of BLDC motors," *Microchip Technology Inc.*, Chandler, AZ, USA, Tech. Rep. cn553863, Apr. 2013.

[30] Z. Salameh and B. Kim, "Advanced lithium polymer batteries," in *Proc. IEEE Power Energy Soc. Gen. Meet.*, 2009, pp. 1–5.

[31] F. Faulhaber, "A second look at gearbox efficiencies," *Mach. Design*, vol. 74, pp. 82–84, Jun. 2002.

[32] A. Ananthanarayanan, M. Azadi, and S. Kim, "Towards a bio-inspired leg design for high-speed running," *Bioinspiration Biomimetics*, vol. 7, no. 4, pp. 1-12, 2012.

[33] K. Rudman, R. Aspden, and J. Meakin, "Compression or tension? The stress distribution in the proximal femur," *BioMedical Eng. OnLine*, vol. 5, no. 1, pp. 1-7, 2006.

[34] T. H. Massie and J. K. Salisbury, "The phantom haptic interface: A device for probing virtual objects," in *Proc. ASME Winter Annu. Meet., Symp. Haptic Interfaces Virtual Environ. Teleoperator Syst.*, 1994, vol. 55, no. 1, pp. 295–300.

[35] R. M. Alexander, "The gaits of bipedal and quadrupedal animals," *Int. J. Robot. Res.*, vol. 3, no. 2, pp. 49–59, 1984.

[36] A. Hill, "The heat of shortening and the dynamic constants of muscle," *Proc. Roy. Soc. London. Series B, Biol. Sci.*, vol. 126, no. 843, pp. 136–195, 1938.

[37] T. A. McMahon, G. Valiant, and E. C. Frederick, "Groucho running," *J. Appl. Physiol.*, vol. 62, no. 6, pp. 2326–2337, 1987.

[38] T. McGeer, "Passive bipedal running," *Proc. Roy. Soc. London., Biol. Sci.*, vol. 240, no. 1297, pp. 107–134, 1990.

[39] K. Sreenath, H.-W. Park, I. Poulakakis, and J. W. Grizzle, "A compliant hybrid zero dynamics controller for stable, efficient and fast bipedal walking on MABEL," *Int. J. Robot. Res.*, vol. 30, no. 9, pp. 1170–1193, 2011.

[40] D. V. Lee and A. A. Biewener, "Bigdog-inspired studies in the locomotion of goats and dogs," *Integrative Comparative Biol.*, vol. 51, no. 1, pp. 190–202, 2011.

Sangok Seok received the B.S. and M.S. degrees from the School of Mechanical and Aerospace Engineering, Seoul National University, Seoul, Korea, in 2002 and 2004, respectively, and the Ph.D. degree in mechanical engineering from the Massachusetts Institute of Technology, Cambridge, MA, USA, in 2014.

He was with the Korean branch of National Instruments as an Applications Engineer and a Marketing Engineer from 2004 to 2009. His research interests include the locomotion of soft body robotics and fast running quadruped robots.

Albert Wang received the B.S. and M.S. degrees from the Department of Mechanical Engineering, Massachusetts Institute of Technology, Cambridge, MA, USA, in 2010 and 2012, respectively, where he is currently working toward the Ph.D. degree in the Biomimetic Robotics Lab.

His research interests include dynamic robot locomotion and actuation systems.

Meng Yee (Michael) Chuah received the B.S. degree in mechanical engineering with a minor in robotics in 2009 from Carnegie Mellon University, Pittsburgh, PA, USA and the M.S. degree in mechanical engineering in 2012 from Massachusetts Institute of Technology, Cambridge, MA, USA, where he is currently working toward the Ph.D. degree in the Biomimetic Robotics Laboratory.

His research interests include developing sensors that are designed for, and integrated structurally into robots to enable intelligent reactions and behaviors.

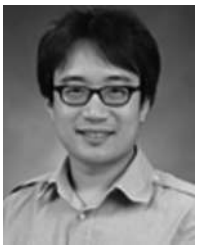

Dong Jin Hyun received the B.S. degree from the School of Mechanical and Aerospace Engineering, Seoul National University, Seoul, Korea, in 2006, the M.S. degree in mechanical engineering from the University of Michigan, Ann Arbor, MI, USA, in 2007, and the Ph.D degree in mechanical engineering from the University of California, Berkeley, CA, USA.

He was the Postdoctoral Associate in mechanical engineering at the Massachusetts Institute of Technology, Cambridge, MA, USA. His research interests include control on wearable robots and dynamics of legged locomotion.

Jongwoo Lee received the B.S. degree in mechanical and aerospace engineering from Seoul National University, Seoul, South Korea, and the M.S. degree in mechanical engineering from Massachusetts Institute of Technology, Cambridge, MA, USA, in 2011 and 2013, respectively.

He is currently a Research Scientist with the Korea Institute of Science and Technology, Seoul, South Korea. His research interests include control and dynamics of legged locomotion, system identification, biomechanics, and wearable robotics.

David M. Otten received the B.S. and S.M. degrees from the Massachusetts Institute of Technology (MIT), Cambridge, MA, USA, in 1973 and 1974, respectively.

In 1974, he joined the MIT Electric Power Systems Engineering Laboratory as a Staff Engineer. Since 1984, he has been a Principal Research Engineer in the renamed Laboratory for Electromagnetic and Electronic System (LEES), MIT. His research interests include instrumentation, power electronics, and the micromouse robot contest.

Jeffrey H. Lang (F'98) received the S.B., S.M., and Ph.D. degrees in electrical engineering from the Department of Electrical Engineering and Computer Science, Massachusetts Institute of Technology (MIT), Cambridge, MA, USA, in 1975, 1977, and 1980, respectively.

He joined the faculty of MIT, in 1980, where he is currently the Vitesse Professor of electrical engineering. He was the Associate Director of the MIT Laboratory for Electromagnetic and Electronic Systems between 1991 and 2003, and as an Associate Editor of Sensors and Actuators between 1991 and 1994. Prof. Lang's research and teaching interests focus on the analysis, design, and control of electromechanical systems with an emphasis on: rotating machinery; micro/nanoscale (MEMS/NEMS) sensors, actuators, and energy converters; flexible structures; and the dual use of electromechanical actuators as motion and force sensors. He has written more than 260 papers and holds 12 patents in the areas of electromechanics, MEMS/NEMS, power electronics, and applied control.

Dr. Lang received the four best-paper prizes from the IEEE societies, and has received two teaching awards from the MIT. He is a coauthor of Foundations of Analog and Digital Electronic Circuits (San Mateo, CA, USA: Morgan Kaufman, 2005), and the Editor of, and a contributor to, Multi-Wafer Rotating MEMS Machines: Turbines Generators and Engines (New York, NY, USA: Springer, 2009).

Sangbae Kim received the B.S. degree in mechanical engineering from Yonsei University, Seoul, South Korea and the Ph.D. degree in mechanical engineering from Stanford University, Stanford, CA, USA, in April 2008.

He is currently an Associate Professor in mechanical engineering at the Massachusetts Institute of Technology (MIT), cambridge, MA, USA. He is the Director of the Biomimetic Robotics Laboratory, MIT. His research interests include design process extracting principles from complex biological systems to achieve technological breakthrough in robotics. He focuses on the convergence of mechanical engineering, control, biology, and material science. His achievement on bioinspired technology development includes the worlds first directional adhesive based on gecko lizards and a climbing robot, called Stickybot, that utilizes the world first synthetic directional adhesives to climb smooth surfaces. His bioinspired climbing robot was selected as one of the best inventions in Time magazine in 2006 and also featured in more than 100 media exposures including Forbes magazine, Wired Science, the History Channel, and the Discovery Channel. He is currently focusing on a cheetah-inspired robotic platform capable of high-speed gallop, employing principles from quadrupedal runners.

Dr. Kim received the DARPA Young Faculty Award 2013 and the NSF Career Award 2014.